Solar Phys (2009) 260: 251–260
DOI 10.1007/s11207-009-9447-1

Nonlinear Evolution of Axisymmetric Twisted Flux Tubes in the Solar Tachocline

R. Hollerbach · P.S. Cally

Received: 2 August 2009 / Accepted: 27 August 2009 / Published online: 3 October 2009
© Springer Science+Business Media B.V. 2009

Abstract We numerically study the evolution of magnetic fields and fluid flows in a thin spherical shell. We take the initial field to be a latitudinally confined, predominantly toroidal flux tube. For purely toroidal, untwisted flux tubes, we recover previously known radial-shredding instabilities, and show further that in the nonlinear regime these instabilities can very effectively destroy the original field. For twisted flux tubes, also including a poloidal component, there are several possibilities, including the suppression of the radial-shredding instability, but also a more directly induced evolution, brought about because twisted flux tubes in general are not equilibrium solutions of the governing equations.

Keywords Interior, tachocline · Instabilities · Magnetohydrodynamics

1. Introduction

The solar tachocline is the transition zone between the uniformly rotating, radiative interior and the differentially rotating convection zone. First discovered helioseismically in the early 1990s, it continues to be probed to this day. Of particular interest is its thinness; the angular-velocity profile changes dramatically over no more than about 5% of the solar radius. This intense shear is one of the reasons why the tachocline is now generally believed to be the seat of the solar dynamo, with poloidal fields being sheared out to produce very strong toroidal fields. See Hughes, Rosner, and Weiss (2007) for reviews of many different aspects of the tachocline, including its role in the solar dynamo.

R. Hollerbach (✉)
Department of Applied Mathematics, University of Leeds, Leeds LS2 9JT, UK
e-mail: rh@maths.leeds.ac.uk

R. Hollerbach · P.S. Cally
Centre for Stellar and Planetary Astrophysics, School of Mathematical Sciences, Monash University, Clayton, Victoria 3800, Australia

P.S. Cally
e-mail: paul.cally@sci.monash.edu.au

Given the combination of strong magnetic fields and shear, it was quickly realized that so-called magneto-shear instabilities could potentially play an important role in the dynamics of the tachocline. Indeed, in other contexts, long before the tachocline was even discovered, it was known that both magnetic fields (Gough and Tayler, 1966) and shear (Watson, 1981) can separately lead to instabilities. The first to study this problem in the tachocline context were Gilman and Fox (1997). A very interesting result obtained by them was that a combination of magnetic fields and shear can be unstable even though each ingredient separately would be stable. Gilman and Fox carried out a two-dimensional calculation, confined to the surface of a sphere with no radial variations allowed. Subsequent work extended this to quasi-three-dimensional shallow-water and three-dimensional thin-shell models, including both linear onset and nonlinear equilibration studies. See Gilman and Cally (2007) for a review of this work.

We will consider a different type of two-dimensionality, namely axisymmetric solutions. These have not received as much attention as some of the three-dimensional solutions, but recent linear-onset calculations (Cally, Dikpati, and Gilman, 2008; Dikpati *et al.*, 2009) indicated that if the toroidal field is concentrated into latitudinal bands, instabilities may arise that shred the field in the radial direction. In this article we consider the nonlinear evolution of such banded fields. For purely toroidal, untwisted flux tubes we obtain results in good qualitative agreement with the linear-onset calculations. For mixed toroidal plus poloidal, twisted flux tubes (which were not considered before) we show that the field evolves not just *via* the onset of instabilities, but much more directly, simply because, in general, it is not an equilibrium solution of the governing equations. For twisted flux tubes there is then a variety of possible outcomes, depending on the strengths of both the toroidal and poloidal components.

2. Equations

The equations we wish to solve are the (Boussinesq) Navier – Stokes equation

$$\frac{\partial \mathbf{v}}{\partial t} + \mathbf{v}\cdot\nabla\mathbf{v} = -\nabla p + (\nabla\times\mathbf{a})\times\mathbf{a} + S\hat{\mathbf{e}}_r + \epsilon\nabla^2\mathbf{v}, \tag{1}$$

the magnetic induction equation

$$\frac{\partial \mathbf{a}}{\partial t} = \nabla\times(\mathbf{v}\times\mathbf{a}) + \epsilon\nabla^2\mathbf{a}, \tag{2}$$

and the entropy equation

$$\frac{\partial S}{\partial t} + \mathbf{v}\cdot\nabla S = -N^2\mathbf{v}\cdot\hat{\mathbf{e}}_r + \epsilon\nabla^2 S. \tag{3}$$

Here $\mathbf{v}$ and $\mathbf{a}$ denote the fluid and Alfvén velocities, respectively, and S the entropy. N is the Brunt – Väisälä frequency, assumed constant. Length was scaled by the inner edge of the tachocline, so we are interested in solving this system in the interval $r \in [1, 1.05]$. Time was scaled by the equatorial rotation frequency; $\mathbf{v}$ and $\mathbf{a}$ scale as length/time.

Except for the inclusion of the diffusive terms ($\epsilon\nabla^2\cdot$), these equations are the same as in Cally, Dikpati, and Gilman (2008), hereafter referred to as CDG08. Some diffusivity must be included here to ensure numerical stability, but values in the range $\epsilon = 10^{-5}$ to 10^{-6}

yielded similar results, indicating that diffusivity is not significantly affecting the evolution. The results presented here are all at $\epsilon = 2 \times 10^{-6}$.

While the equations may be much the same, the subsequent analysis is very different from that of CDG08. They considered only the linear onset of instability, and only for high radial wavenumber (k), thereby ultimately eliminating r entirely, instead simply having k as a parameter in the equations. In contrast, we are interested in a direct numerical solution in the finite interval $r \in [1, 1.05]$, allowing an arbitrary radial dependence, and also including the full nonlinear evolution of the solutions.

For axisymmetric solutions, it is convenient to decompose $\mathbf{v}$ and $\mathbf{a}$ as

$$\mathbf{v} = v\hat{\mathbf{e}}_\phi + \nabla \times (\psi \hat{\mathbf{e}}_\phi), \qquad \mathbf{a} = b\hat{\mathbf{e}}_\phi + \nabla \times (a\hat{\mathbf{e}}_\phi). \tag{4}$$

The toroidal parts, v and b, are the azimuthal components of the given vectors; the poloidal parts, ψ and a, are the streamfunctions of the meridional components. The original Equations (1) and (2) then become

$$\frac{\partial}{\partial t} v = P_1(b, a) - P_1(v, \psi) + \epsilon D^2 v, \tag{5}$$

$$\frac{\partial}{\partial t} D^2 \psi = \frac{1}{r} \frac{\partial}{\partial \theta} S + P_2(b, b) + P_2\big(D^2 a, a\big) - P_2(v, v) - P_2\big(D^2 \psi, \psi\big) + \epsilon D^4 \psi, \tag{6}$$

$$\frac{\partial}{\partial t} b = P_2(v, a) - P_2(b, \psi) + \epsilon D^2 b, \tag{7}$$

$$\frac{\partial}{\partial t} a = P_1(\psi, a) + \epsilon D^2 a, \tag{8}$$

where

$$D^2 = \nabla^2 - 1/(r \sin\theta)^2, \tag{9}$$

and

$$P_1(X, Y) = \hat{\mathbf{e}}_\phi \cdot \big[\big(\nabla \times (X\hat{\mathbf{e}}_\phi)\big) \times \big(\nabla \times (Y\hat{\mathbf{e}}_\phi)\big)\big], \tag{10}$$

$$P_2(X, Y) = \hat{\mathbf{e}}_\phi \cdot \nabla \times \big[(X\hat{\mathbf{e}}_\phi) \times \big(\nabla \times (Y\hat{\mathbf{e}}_\phi)\big)\big]. \tag{11}$$

We then wish to solve Equations (5) and (6) with stress-free boundary conditions

$$\frac{\partial}{\partial r}\left(\frac{v}{r}\right) = \psi = \frac{\partial^2}{\partial r^2}\psi = 0 \quad \text{at } r = 1, 1.05, \tag{12}$$

Equations (7) and (8) with perfectly conducting boundary conditions

$$\frac{\partial}{\partial r}(br) = a = 0 \quad \text{at } r = 1, 1.05, \tag{13}$$

and Equation (3) with $S = 0$ at $r = 1, 1.05$. These boundary conditions are somewhat artificial, but *any* boundary conditions would necessarily be artificial. To properly capture all of the dynamics of the tachocline it should not be studied in isolation, but rather as part of a global model that also includes the interior and the convection zone. However, while there are models that aim in this direction (Brun and Toomre, 2002), they are so complicated that aspects such as tachocline instabilities cannot be specifically focused on. In order

to study tachocline instabilities simplified models such as ours must be adopted, despite the inevitably unnatural boundaries where the real Sun has none.

We solve these equations using the numerical code described by Hollerbach (2000), in which the radial structure is expanded in terms of Chebyshev polynomials, the angular structure in terms of spherical harmonics, and the time-stepping is done *via* a second-order Runge – Kutta method. Resolutions ranging from 50×1600 to 80×2400 in (r, θ) were used, and were all checked to ensure that the results were adequately resolved. A timestep of 10^{-3} was sufficiently small to ensure stability.

To facilitate comparison with CDG08, we choose initial conditions much the same as theirs. The initial entropy is simply $S = 0$, so any buoyancy effects arise entirely out of the subsequent evolution. For the flow, we take the solar-like differential-rotation profile $\omega = v/(r \sin\theta) = 1 - 0.18 \cos^2\theta$, where we note that Equation (1) is written in a non-rotating frame, so ω here must include an overall rotation, not just the Pole-to-Equator differential rotation $-0.18 \cos^2\theta$.

For the toroidal field, we take

$$b = Ap\left[\mathrm{e}^{-4(\mu-d)^2/W^2(1-d^2)} - \mathrm{e}^{-4(\mu+d)^2/W^2(1-d^2)}\right] \sin\theta/r, \tag{14}$$

where $\mu = \cos\theta$. That is, b consists of two oppositely directed bands in the two hemispheres, with position d, latitudinal bandwidth W, and amplitude A. The normalization factor p is adjusted such that the maximum field strength ($\max_\theta(b)$) is $A/2$.

Values of A up to 1, corresponding in dimensional terms to $\max_\theta(b) \approx 10^5$ G, are of greatest interest in the solar context, but other (especially younger) solar-type stars may well have even larger values. We will present runs for $A = 1$ and 2. A range of possibilities for d and W were considered and yielded qualitatively similar results. We therefore show results only for $d = 0.5$, corresponding to bands situated $\pm 30°$ from the Equator, and $W = \pi/36$, corresponding to a bandwidth of 5°.

Thus far our initial conditions are exactly as in CDG08; see also Dikpati and Gilman (1999) who were the first to introduce banded toroidal fields of this type. To this toroidal field, we now add the poloidal field

$$a = A' p'\left[\mathrm{e}^{-4(\mu-d)^2/W^2(1-d^2)} + \mathrm{e}^{-4(\mu+d)^2/W^2(1-d^2)}\right] \sin\theta (r-1)(r-1.05). \tag{15}$$

Thus the poloidal field has the same banded structure as the toroidal, but a is equatorially symmetric, whereas b is anti-symmetric. Both of these symmetries correspond to the standard "dipole" solutions of solar dynamo theory. The differing radial dependencies, $(r-1)(r-1.05)$ for a *versus* $1/r$ for b, are dictated by the different boundary conditions of Equation (13) that a and b are supposed to satisfy. The normalization factor p' is adjusted such that $\max_\theta(a)$ is A'.

The amplitude $A' = fA$, so the factor f gives the ratio of poloidal to toroidal fields. In addition to the $f = 0$ untwisted flux tubes, we will take $f = \pm 10^{-4}$ and $\pm 4 \times 10^{-4}$ for the twisted flux tubes. The sign of f determines whether the tubes are twisted in a left- or right-handed sense. It is not certain which is more appropriate to the tachocline (Fan, 2004) so we consider both possibilities, and show that they yield qualitatively similar behavior. Regarding the amplitudes of f, for $A = 1$ and $|f| = 10^{-4}$, the maximum values of (a_r, a_θ, a_ϕ) are $(0.0022, 0.0092, 0.5)$. Even for $|f| = 4 \times 10^{-4}$ the field is thus predominantly azimuthal, with only around one twist over the full circumference $\phi \in [0, 2\pi]$. We will see though that even such relatively weak poloidal fields as this can significantly influence the subsequent evolution.

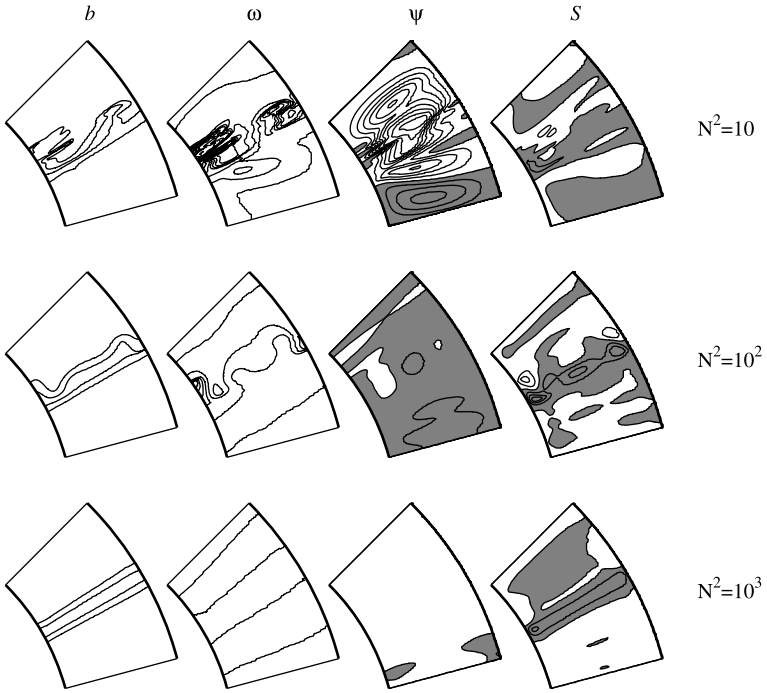

Figure 1 From left to right, contours of b, ω, ψ, and S, with contour intervals of 0.2, 0.02, 5×10^{-5}, and 0.1, respectively. In the plots for ψ and S, gray denotes positive values, white negative ($\psi > 0$ corresponds to clockwise circulation). From top to bottom, the three rows are for $N^2 = 10, 10^2$, and 10^3. $A = 1$ and time $t = 5$ for all three. The range of r is 1 to 1.05, but has been stretched by a factor of ten, and hence looks like 1 to 1.5.

3. Results

3.1. Untwisted Flux Tubes

We begin by considering the influence of the stratification. Figure 1 shows results for $N^2 = 10, 10^2, 10^3$, all for $A = 1$ and $f = 0$. Within each row, the first panel shows the toroidal field b, the second panel the angular velocity $\omega = v/(r \sin\theta)$, the third the meridional circulation ψ, and the fourth the entropy S. (According to Equation (8), if $a = 0$ initially, it will remain zero.) Only the range $\theta \in [45°, 75°]$ is shown, centered on the flux tube at $\theta = 60°$. The radial direction was stretched by a factor of 10, that is, the actual gap $r \in [1, 1.05]$ was stretched to look like $[1, 1.5]$.

Turning to the variation with N^2, we see that for $N^2 = 10$ the solution has changed significantly from its initial condition, whereas for $N^2 = 10^3$ it is almost unchanged. The reason for this is easy to understand. If initially only b and v are nonzero – and if a is always zero – then according to Equations (5) and (7), the only way (apart from the very weak dissipation) for either b or v to change is by inducing a meridional circulation ψ. Now, according to Equation (6), the terms $P_2(b, b) - P_2(v, v)$ will indeed induce such a circulation; these terms are zero only if $\frac{\partial}{\partial z}(b^2 - v^2) = 0$, which in general is not the case. However, for increasingly strong stratification, the buoyancy term $(r^{-1}\frac{\partial S}{\partial \theta})$ can very effectively suppress the tendency to drive a meridional circulation. That is, having only b and v nonzero is not quite

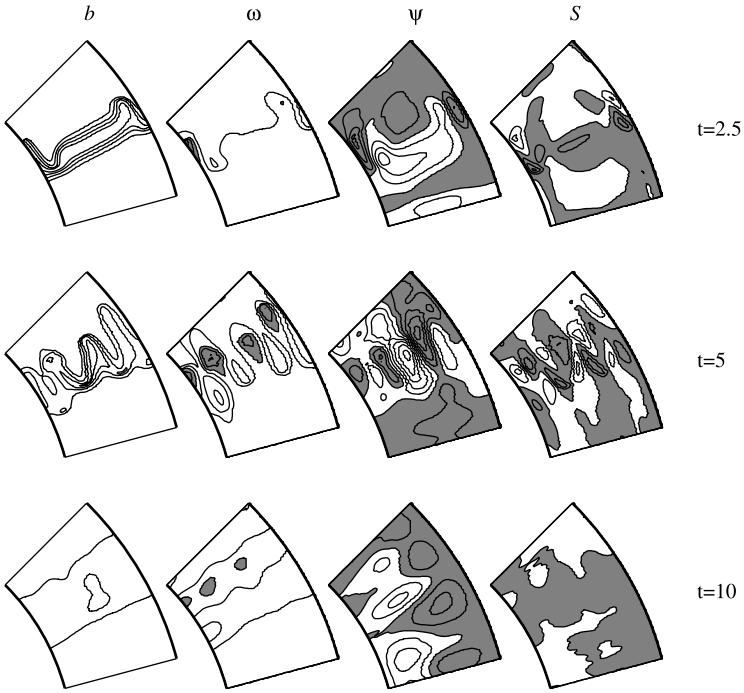

Figure 2 From left to right, contours of b, ω, ψ, and S, with contour intervals of 0.2, 0.05, 5×10^{-5}, and 1, respectively. In the plots for ω, gray indicates regions where $\omega > 1$; for ψ and S, gray denotes positive values, as in Figure 1. $N^2 = 10^3$, $A = 2$, and from top to bottom $t = 2.5$, 5, and 10.

an equilibrium solution to the governing equations, but if N^2 is sufficiently large, only a very weak circulation ψ will be induced. Thus, according to Equations (5) and (7), b and v will remain almost unchanged. This justifies linear-stability analyses such as those of CDG08, where a basic state is simply imposed for b and v. In the remainder of this article we will consider only the strongly stratified case $N^2 = 10^3$.

Figure 2 shows the effect of doubling the field strength to $A = 2$. Now even the strong stratification is not enough to stabilize the solution. Instead, we see the development of precisely the radial-shredding instabilities previously studied by CDG08. Here though we follow the full nonlinear evolution, and discover that by $t = 10$ the instability has almost completely obliterated the original flux tube.

3.2. Twisted Flux Tubes

Figures 3 and 4 show the results for $A = 1$ and $f = \pm 4 \times 10^{-4}$. That is, the amplitude $A = 1$ is as in Figure 1, too low for the shredding instability to occur, and indeed it does not. Nevertheless, the solutions also do not remain virtually stationary, as in the bottom row in Figure 1. Instead, we see the development of highly localized jets in the angular velocity ω. To understand their origin, we return to Equation (5), where the term $P_1(b, a)$ is clearly responsible; this term is zero only if contours of b and a coincide, which in general is not the case. Furthermore because there is no buoyancy force in this equation, no amount of stratification can suppress this effect, very much unlike Figure 1.

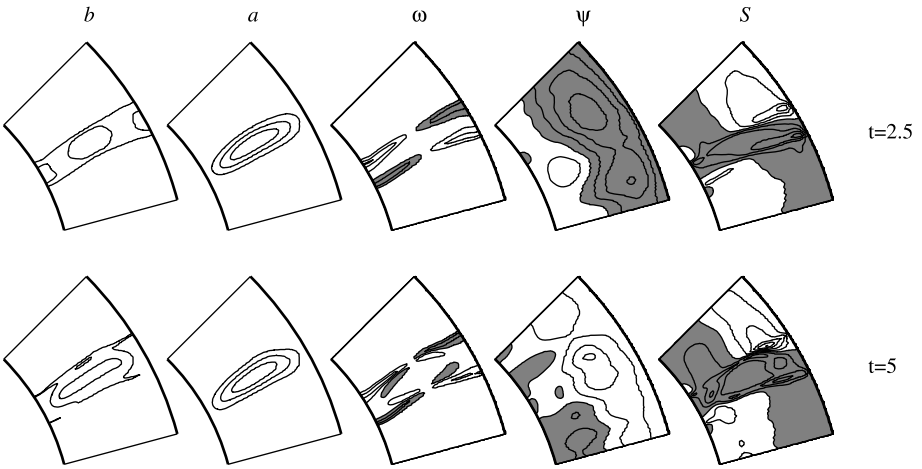

Figure 3 From left to right, contours of b, a, ω, ψ, and S, with contour intervals of 0.2, 10^{-4}, 0.1, 2×10^{-5}, and 0.2, respectively. In the plots for ω, gray indicates regions where $\omega > 1$; for ψ and S, gray denotes positive values, as in Figure 1. $N^2 = 10^3$, $A = 1$, and $f = 4 \times 10^{-4}$, corresponding to clockwise circulation for the poloidal field. The top row is at $t = 2.5$, the bottom row at $t = 5$.

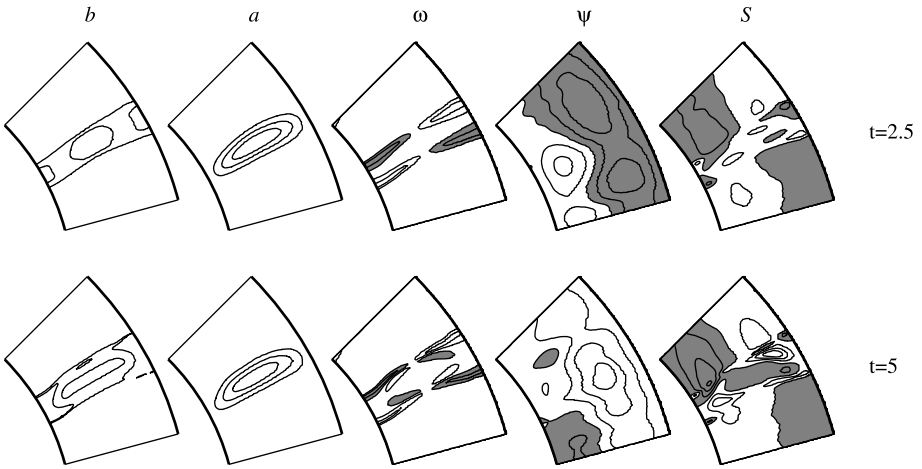

Figure 4 From left to right, contours of b, a, ω, ψ, and S, with contour intervals of 0.2, 10^{-4}, 0.1, 2×10^{-5}, and 0.2, respectively. $N^2 = 10^3$, $A = 1$, and $f = -4 \times 10^{-4}$, corresponding to counter-clockwise circulation for the poloidal field. (Incidentally, it is perhaps explicitly worth noting that because of the ten-fold stretching in the radial direction, a_θ is actually ten times greater than the spacing of the contour levels might suggest. So in fact a_θ is greater than a_r.)

Comparing Figures 3 and 4 in detail, we note that reversing the sign of a (that is, the sense of twist in the tube) has exactly the effect that one might expect; reversing the sign of $P_1(b, a)$ simply reverses the jets. Otherwise the evolution is much the same, and in both cases the flux tubes largely maintain their strength. Note also that jets as concentrated as this would not be detectable by helioseismology, so phenomena such as these could conceivably exist in the real tachocline.

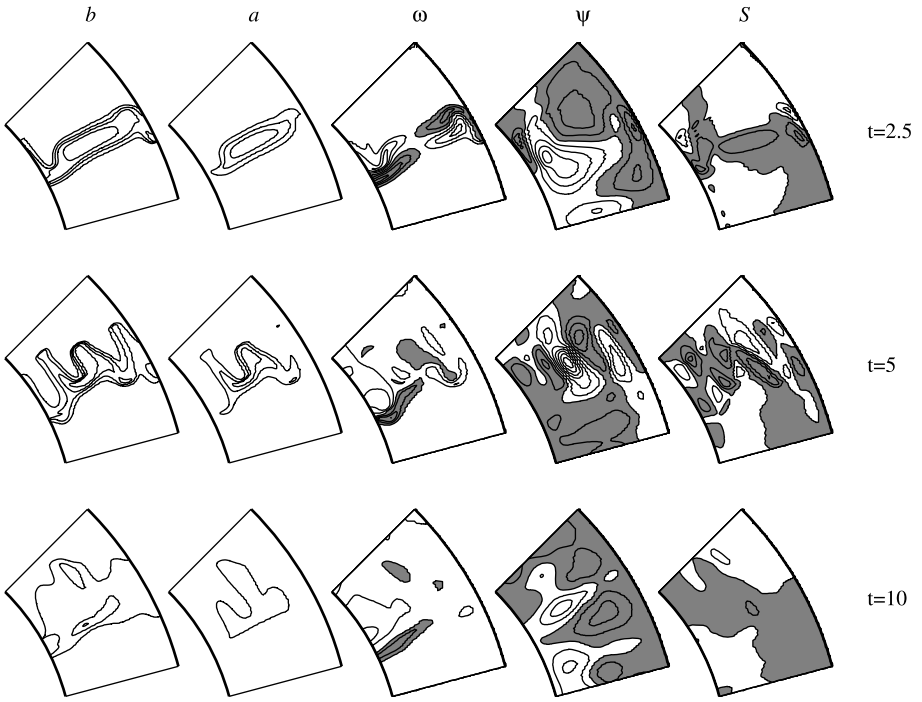

Figure 5 From left to right, contours of b, a, ω, ψ, and S, with contour intervals of 0.2, 5×10^{-5}, 0.1, 5×10^{-5}, and 1, respectively. In the plots for ω, gray indicates regions where $\omega > 1$; for ψ and S, gray denotes positive values. $N^2 = 10^3$, $A = 2$, and $f = 10^{-4}$. From top to bottom $t = 2.5$, 5, and 10.

Figure 5 shows results for $A = 2$ and $f = 10^{-4}$. The toroidal field is therefore as in Figure 2, whereas the poloidal field is half as strong as in Figure 3 (so the nonlinear term $P_1(b, a)$ is just as strong as in Figure 3). Initially we see the same jets as in Figures 3 and 4 (and reversing the sign of f again merely reverses the jets). By $t = 5$ the evolution is dominated by the same shredding instability as in Figure 2, and the final result is much the same, with the original flux tube largely destroyed. Poloidal fields as weak as this, therefore, have relatively little influence. However, if we increase the poloidal field strength to $f = 4 \times 10^{-4}$, it does have a very significant influence, as illustrated in Figure 6. The radial-shredding instability is now completely suppressed, and the flux tube persists up to $t = 10$ (and beyond). Note also how the solution has adjusted itself so that contours of b and a largely do coincide now, and correspondingly these localized jets are greatly reduced in strength.

4. Conclusions

We consider the evolution of flux tubes in a thin spherical shell, intended to model solar-type tachoclines. For untwisted tubes we obtain the same radial-shredding instabilities that were previously studied in the linear regime, and show that in the nonlinear regime these instabilities can very efficiently destroy the original flux tube simply by shredding it to sufficiently short length-scales for it to dissipate.

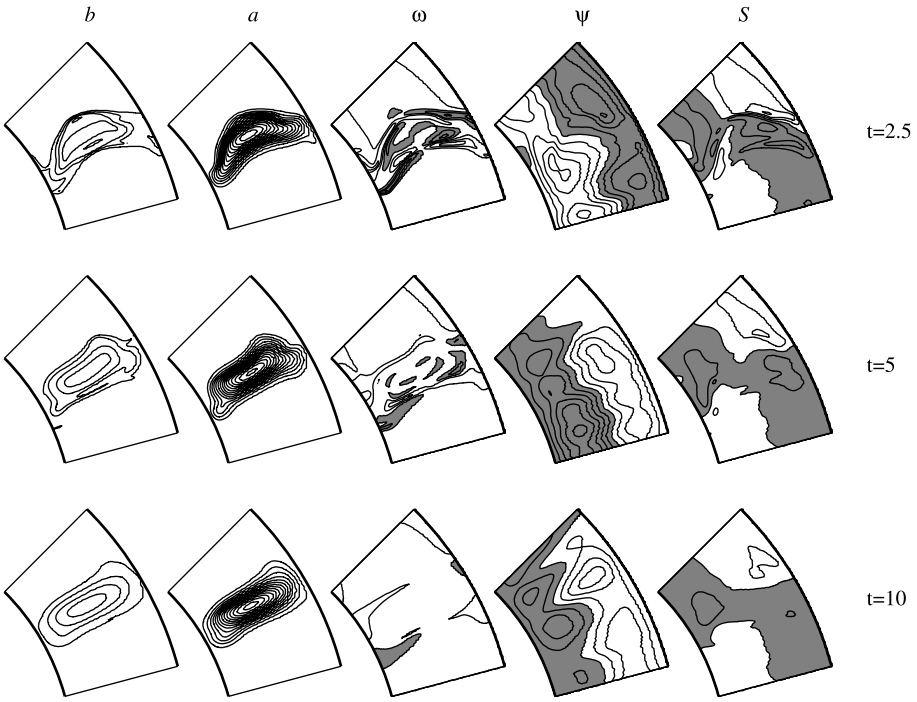

Figure 6 From left to right, contours of b, a, ω, ψ, and S, with contour intervals of 0.2, 5×10^{-5}, 0.1, 5×10^{-5}, and 1, respectively. In the plots for ω, gray indicates regions where $\omega > 1$; for ψ and S, gray denotes positive values. $N^2 = 10^3$, $A = 2$, and $f = 4 \times 10^{-4}$. From top to bottom $t = 2.5$, 5, and 10.

For twisted flux tubes, there are a number of possibilities. If the toroidal field is too weak for instabilities to set in, the solution will nevertheless evolve, *via* the formation of differential-rotation jets, driven directly by the Lorentz forces associated with the twist in the tube. These jets induce a certain amount of structure in the flux tubes, but not enough to disrupt it as did the instabilities. If the toroidal field is sufficiently strong, and the poloidal field very weak, the shredding instabilities develop much as before, and simply overwhelm the jets driven by the twist. Finally, if the poloidal field is somewhat stronger – but still much weaker than the toroidal – it can suppress the shredding instability. Twisted flux tubes can therefore exist at considerably greater field strengths than untwisted tubes.

Future work will extend this model to three dimensions and study the interaction of some of the effects presented here with some of the previously known non-axisymmetric magneto-shear instabilities (Gilman and Cally, 2007).

Acknowledgements This work was supported by the UK Science and Technology Facilities Council Grant No. PP/E001092/1. RH's visit to Australia was supported by a Royal Society International Travel Grant.

References

Brun, A.S., Toomre, J.: 2002, *Astrophys. J.* **570**, 865.
Cally, P.S., Dikpati, M., Gilman, P.A.: 2008, *Mon. Not. Roy. Astron. Soc.* **391**, 891 (CDG08).
Dikpati, M., Gilman, P.A.: 1999, *Astrophys. J.* **512**, 417.

Dikpati, M., Gilman, P.A., Cally, P.S., Miesch, M.S.: 2009, *Astrophys. J.* **692**, 1421.
Fan, Y.: 2004, *Living Rev. Solar Phys.* **1** (cited on 1 August 2009). http://www.livingreviews.org/lrsp-2004-1.
Gilman, P.A., Cally, P.S.: 2007, In: Hughes, D., Rosner, R., Weiss, N. (eds.) *The Solar Tachocline*, Cambridge University Press, Cambridge, 243.
Gilman, P.A., Fox, P.A.: 1997, *Astrophys. J.* **484**, 439.
Gough, D.O., Tayler, R.J.: 1966, *Mon. Not. Roy. Astron. Soc.* **133**, 85.
Hollerbach, R.: 2000, *Int. J. Numer. Methods Fluids* **32**, 773.
Hughes, D., Rosner, R., Weiss, N. (eds.): 2007, *The Solar Tachocline*, Cambridge University Press, Cambridge.
Watson, M.: 1981, *Geophys. Astrophys. Fluid Dyn.* **16**, 285.